Numerical simulation of flame instability in lean H_2/air mixtures

J.F. Yu*, R. Yu, and X.S. Bai
Jiangfei.Yu@energy.lth.se
Division of Fluid Mechanics, Lund University, 22100 Lund, Sweden

Abstract
This paper reports on studies of the instability of lean hydrogen/air laminar premixed flames with the equivalence ratio of 0.6. Two intrinsic instability mechanisms are involved in the flames, hydrodynamic instability and thermal-diffusive instability. Numerical simulations employing detailed chemical kinetics and transport properties are carried out to simulate the initial linear growth of instability as well as the nonlinear evolution of flame instability under two different pressures, 5 atm and 25 atm. A small perturbation of sine wave with a prescribed wavelength and small amplitude is first placed on the initial planar laminar flame front. Then, the evolution of the sine wave shaped flame front is simulated. Chaotic flame fronts are captured whose nonlinear evolution is shown to be very sensitive to initial perturbations. In the initial linear growth stage, the amplitude of the initial sine wave flame front grows exponentially. Later on, the flame front develops into wrinkling surface with different wavelengths and amplitudes. Preference of cellular flame cells with even or odd modes has been observed which is keen on initial perturbation with small wave numbers. With smaller even number of waves in the initial perturbation of the flame front, e.g. six waves, the even wave modes are amplified and odd wave modes are suppressed; whereas, with bigger number of initial waves, e.g. eleven waves, the even and odd wave modes can compete fairly with each other. After a long time, the long wavelength mode dominates. In high-pressure flames, the flames are thinner, both of hydrodynamic and thermal-diffusive instability are enhanced, and the flame fronts are more chaotic.

Introduction

Intrinsic flame instability is a phenomenon frequently seen in laminar flames [1-6], e.g. in flames with non-unity Lewis numbers. It has implication in engineering applications, e.g. safety in nuclear power plants [1]. There are several mechanisms of intrinsic flame instability: the hydrodynamic instability (also known as Landau-Darrieus (LD) instability) induced by thermal expansion from exothermal reactions [2, 3], thermal-diffusive (TD) instability owing to differential diffusion between thermal diffusion and mass diffusion [4, 5], and Rayleigh-Taylor instability (with a larger scale) due to buoyancy force. Without considering turbulence and body force, hydrodynamic instability and thermal-diffusive instability result in multi-dimensional unstable cellular shaped flames frequently. These have been observed in the experiments and have been reviewed by several researchers [7-11].

Formation of cellular flame from an initial planar flame has been studied theoretically. Usually a dispersion relation is found from linear stability analysis, which states the influence of parameters contained in models on stability at the linear stage of flame evolution. Considering both instabilities, hydrodynamic and thermal-diffusive, the analyses based on asymptotic linear stability theories assuming high activation energy have been performed [12-16]. Recently, finite activation energy linear stability analyses have been carried out [17-19], which provide conditions closer to reality. Beyond the onset of instability, linear stability theories fail to simulate the flame front evolution. Weakly nonlinear flame front evolution theories with asymptotic limits of high activation energy have been developed by Sivashinsky et al., e.g. Kuramoto–Sivashinsky (KS) equation containing purely thermal-diffsive nature,

Michelson–Sivashinsky (MS) equation accommodating purely hydrodynamic instability, and for a mixed problem, a third equation which combined by the KS and MS equations [20]. These equations are solved using numerical methods to study the nonlinear evolution of flame [21-23]. MS equation has been extended to higher order models [24, 25].

Numerical simulations of the nonlinear evolution of flame have been carried out by solving full Navier-Stokes (NS) equations for either compressible flows [26-29] with one- or two-step reaction chemistry models, or incompressible flows [30-32] with detailed chemistry model, in order to capture cellular instability more accurately, and to examine and develop linear and nonlinear theoretical models. The approach is used in this work.

Complex flame dynamics is invoked by hydrodynamic instability, damped or enhanced by thermal-diffusive instability whose key parameter is the effective Lewis number, or equivalently, effective Markstein number [11]. For premixed mixture of subunity Lewis number, e.g. H_2/air, detailed numerical simulations performed with one- or two-step reaction chemistry models [26-29] have shown very intense nonlinear behaviors of flames including cell-merging and splitting, symmetry breaking bifurcation, local quenching and cell lateral movement.

Only a few numerical simulations have been performed with detailed chemistry mechanisms and transport properties with subunity Lewis number [32-34], where Soret effect [33] and turbulence effect [34] are studied. Altantzis et al. [32] used low Mach number code with spectral element method and Li's detailed H_2 chemistry [35] model to simulate 2D planar lean premixed H_2/air flames. They reported the results of linear instability, the influence of width of computational domain on the nonlinear flame front evolution, and the behavior of flame front in a wide domain. The results show that TD instability is increased with larger domain width.

In this work, we investigate the nonlinear evolution of 2D planar lean H_2/air premixed flame in a wide region which can correctly predict multicell interaction, validated by Yuan et al. [26]. This is motivated by the fact that systematic and general interpretation has not established yet in the nonlinear evolutions of flame fronts with coupling LD instability and TD instability. In addition, we consider the long time evolution of flame front at the condition of high pressure.

The content of this paper is as follows: Firstly, the computational setup is presented. The simulation case is similar to the one of large computational domain [32]. Results are analyzed and compared with the previous results of [32]; then high pressure case is simulated and pressure dependence is investigated; finally, dependence of flame instability on the initial perturbation is studied.

Numerical methods

Laminar lean hydrogen/air premixed flame propagation in a two-dimensional domain is considered. The flow speed is low and essentially it can be assumed as low Mach number flow. The physical pressure can be decomposed into two parts, one thermodynamic pressure that is uniform throughout the cylinder and one hydrodynamic pressure that appears in the momentum equation. The mixture considered is in gas phase, without body force, and with negligible thermal radiation. The governing equations are made up of the transport equations of species mass fraction and energy, the Navier-Stokes equations, and the continuity equation,

$$\rho \frac{DY_k}{Dt} = -\frac{\partial \rho V_{k,i} Y_k}{\partial x_i} + \dot{\omega}_k \tag{1}$$

$$\rho \frac{Du_i}{Dt} = -\frac{\partial p}{\partial x_i} + \tau_{ij} \tag{2}$$

$$\rho C_p \frac{DT}{Dt} = -\sum_{k=1}^{N} h_k \dot{\omega}_k - \left(\rho \sum_{k=1}^{N} C_{p,k} Y_k V_{k,i} \right) \frac{\partial T}{\partial x_i} + \frac{\partial P}{\partial t} + \frac{\partial}{\partial x_i} \left(\lambda \frac{\partial T}{\partial x_i} \right) \tag{3}$$

$$P = \rho RT \sum_{k=1}^{N_{sp}} \frac{Y_k}{W_k} \tag{4}$$

$$\frac{\partial u_i}{\partial x_i} = -\frac{1}{\rho} \frac{D\rho}{Dt} \tag{5}$$

where ρ is density; Y_k is mass fraction of species k; u_i is the velocity component in the x_i-direction; $V_{k,i}$ is the diffusion velocity of species k in the x_i-direction; $\dot{\omega}_k$ is the net formation rate of species k; p is the hydrodynamic pressure; P is the thermodynamics pressure; τ_{ij} is the component of viscous stress tensor; h_k is the specific enthalpy of species k; $C_{p,k}$ is the specific heat capacity of species k at constant pressure; T is temperature; λ is thermal diffusivity; W_k is the molecular weight of species k. DT/Dt denotes the material derivative of temperature.

The continuity equation is deliberately written in terms of the material derivative of density, which then make use of the equation of state (4) to link the continuity equation with the species transport equation (1) and the energy transport equation (3). In this way, robust numerical stability can be achieved when high density gradients exist in the flow field [36].

The fractional step method [36] is used in the numerical solution of the above governing equations. Based on the operator split method the numerical integration of species and energy equations are performed in two steps, first a reacting step where chemical reaction rates and heat release rates are integrated using a stiffness solver with detailed chemistry, and then an advection-diffusion step where advection and molecular diffusion terms are integrated. In this method most variables can be computed explicitly or semi-explicitly except the hydrodynamic pressure, which is obtained from solution of a variable coefficient Poisson equation derived from the momentum equations and the continuity equation. The pressure equation is solved using a multi-grid method [37, 38]. The solver is parallelized based on domain decomposition.

The spatial derivatives in the governing equations are discretized using 6th order central difference scheme. The advection terms in the species transport and energy transport equations are discretized using a 5th order WENO scheme [39] to avoid wiggles in species mass fractions that can lead to unphysical solution. The time integration is done using 1st order Euler explicit scheme. Variable time stepping size is determined by satisfying both advection and diffusion stability limits. More details of the solver and numerical methods can be found in [40].

Computational cases, initial and boundary conditions

The computation is carried out in a two-dimensional rectangular domain, with a size of $160\delta_L$ and $80\delta_L$ along respectively streamwise (x-direction) and laterally (y-direction), where δ_L is the thickness of laminar unstretched planar flame under the corresponding condition. Table 1 lists the initial condition of the mixture and the computational parameters. Two cases are studied, one with a 5 atm pressure and one with an elevated pressure of 25 atm. In both cases the equivalence ratio is set to 0.6, and temperature of the unburned mixture 298 K. The chemical kinetic mechanism for H_2/air mixture is the H_2 subset of the Peters' mechanism [41], which contains 9 species and 19 reactions. Based on this mechanism and the present numerical method a one dimensional unstretched planar flame calculation is performed under the conditions of case A and B to determine the reference laminar flame thickness and laminar flame speed (S_L). The laminar flame thickness is defined based on the maximum gradient of temperature profile,

$$\delta_L = (T_b - T_u) \Big/ \left(\frac{dT}{dx} \right)_{\max} \tag{6}$$

where T_b and T_u are the temperatures of the combustion products and unburned mixture respectively. The results are given in Table 1. Case B with higher pressure has a thinner flame and slower flame speed than case A.

A uniform grid with a mesh size (h) one eighth of δ_L is employed. Periodic condition is adopted at the lateral boundaries. The streamwise flow velocity at the upstream boundary is set to the flame speed; at downstream boundary a zero gradient of dependent variables is used as the outflow condition. Some authors used symmetric conditions in the lateral boundaries, as was shown to prohibit cells to move in the lateral direction [28, 29].

Table 1. Initial condition and computational cases

Cases	ϕ	T_0 [K]	P_0 [atm]	S_L [m/s]	δ_L [μm]	h/δ_L	grids
A	0.6	298	5	0.395	86	1/8	1280×640
B	0.6	298	25	0.073	66	1/8	1280×640

As the initial condition, a planar flame from the corresponding 1D flame simulation is placed in the middle of the domain. An infinitesimal sinusoidal disturbance $A\sin(2\pi ny/L)$ is made at the flame front in transverse (y) direction, where A is the amplitude and n is the wave number of sinusoidal disturbance. In the present study A is set to $0.1\delta_L$ and n is set to 6 or 11 to examine the sensitivity of flame instability to the initial disturbance.

Case A: lean H_2/air flame at 5 atm

Figure 1 shows instantaneous field of OH mass fraction and temperature at five critical instances of time. Six waves have been placed at the initial flame front. The time has been non-dimensionalized by δ_L/S_L, which is the characteristic time of the corresponding laminar planar flame. Figure 2 shows the flame front in the earlier evolution stage. The flame front is defined as the iso-contour with the value where the gradient of temperature is at its maximum in corresponding 1D flame. As seen in Fig.1a and Fig.2, the initial perturbation at the flame front grows exponentially until $t^*=tS_L/\delta_L=4$. The flame front changes to a cellular shape as it evolves. The leading front protruding to the unburned side remains smooth (low positive curvature) with higher temperature and higher OH mass fraction, whereas the trailing edge of the flame front becomes nearly cusp-shape (high negative curvature) with lower temperature and lower OH mass fraction. This is owing to the well-known thermal-diffusive instability of lean hydrogen/air flame: at the leading front the equivalence ratio becomes higher due to faster diffusion of hydrogen as compared to other species and heat; at the trailing edge the equivalence ratio is lower due to the clustering and subsequent consumption of hydrogen at the leading front.

Until t^*=4, the wavelength of the wrinkled flame front remains essentially the same as that at the initial disturbance, i.e. six waves shown in Figs.1a and 2a. This period is often referred to as linear growth period. Thereafter, some flame front cells tend to merge together to form a larger cell, and at the same time some cells split to smaller ones, cf. Figs.1b-1d. To analyze the length scales of the cells a Fourier analysis of the flame front function $x=f(y)$ is made. The wavelengths $\lambda_k=L/k$ (k=1, 2, 3 …) and its associated amplitude A_k are identified, where k is the wave number associated with the wavelength λ_k (in a conventional sense, k/L is the wave number), which would be the number of waves within the lateral direction of the computational domain if the wave had a single wavelength λ_k. As seen in Fig.2b, after t^*=3 cells with k=10 (k_{10}) start to grow, indicating splitting of the k_6 cells to smaller cells. After

t^*=4, the larger cells with k=4 (k_4) start to grow, owing to merging of the k_6 cells to larger ones. In the period of 4<t^*<5, the amplitude of original k_6 cells decreases due to splitting of the cells to smaller ones and merging to larger cells.

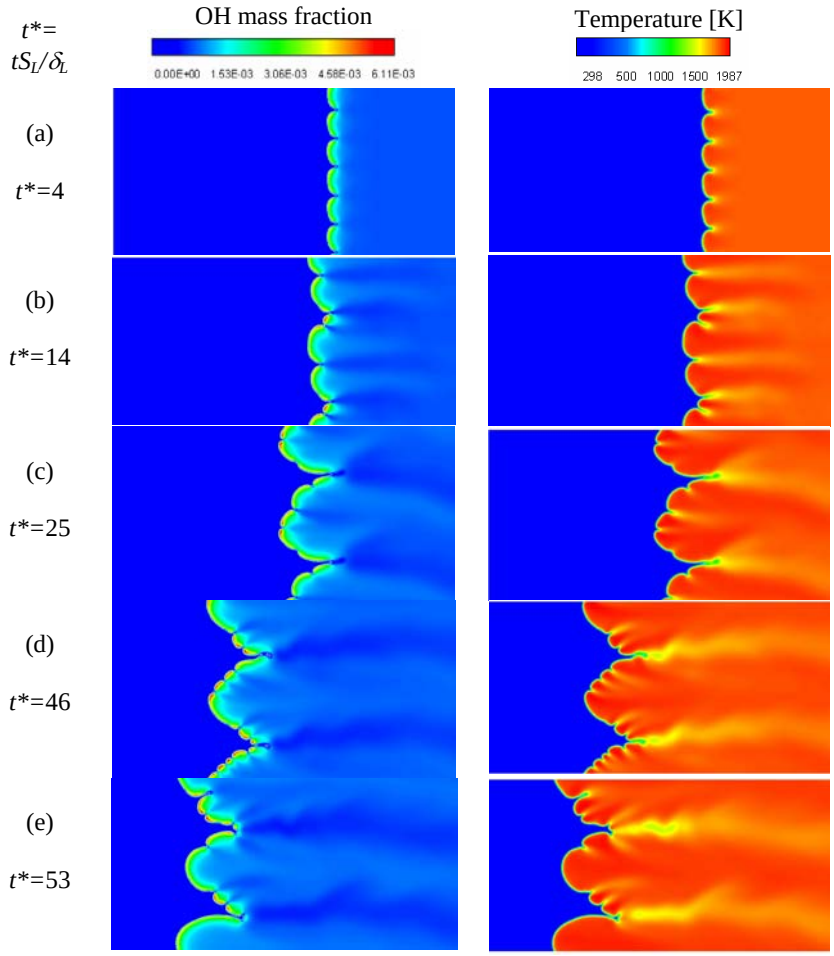

Figure 1. Instantaneous field of OH mass fraction and temperature showing five critical instances of time for case A. (a) at the end of the linear growth stage, (b) at the instance that larger cells with k=2 become dominant, (c) at the instance that cells with odd wave number appear, (d) at the instance that cells with odd wave number start to grow rapidly.

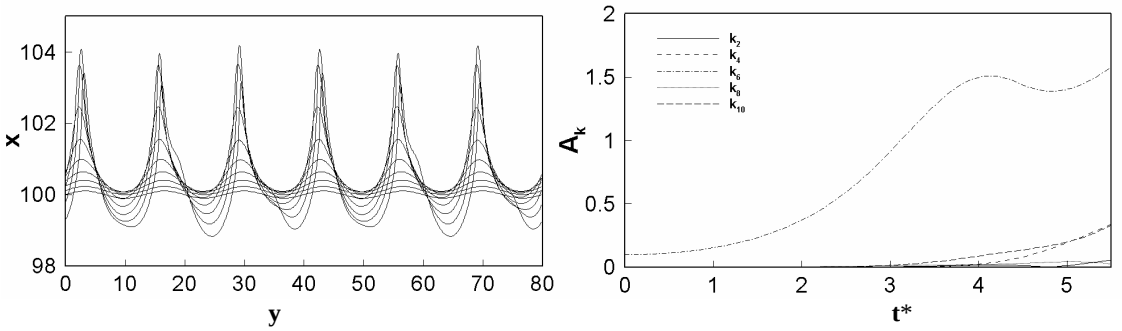

Figure 2. (a) Evolution of the flame front at the linear growth period, (b) amplitude of the flame front cells at different wave numbers as a function of time. The initial pressure is 5 atm; the initial disturbance at the flame front has a wave number of 6.

Figure 3 shows the splitting and merging of cells during a longer period of time $t^*<53$. It is interesting to note that the odd wave number cells do not appear until $t^*=25$, whereas the even wave number cells appear much earlier. The amplitude of the larger cells (k=1, k=2) grows quickly initially. At $t^*=14$, the k_2 cells (k=2) overtake the k_4 cells to become the largest, cf. Fig.1b. After $t^*=20$ the even wave number cells appear to be in statistical quasi stationary, in the sense that the cell amplitudes oscillate around their corresponding mean ones. The mean amplitudes are smaller for cells with larger wave numbers. The odd wave number cells have a similar behavior as the even wave number cells, although there is a delay in time for the cells to become statistical stationary. Of particular interest is the rapid growth of k_1 cells after $t^*=46$. Several authors [26, 32] reported that after long time evolution the k_1 cells become dominant. The long wavelength cells are formed due to hydrodynamic instability whereas the small wavelength cells are owing to thermal-diffusive instability [1].

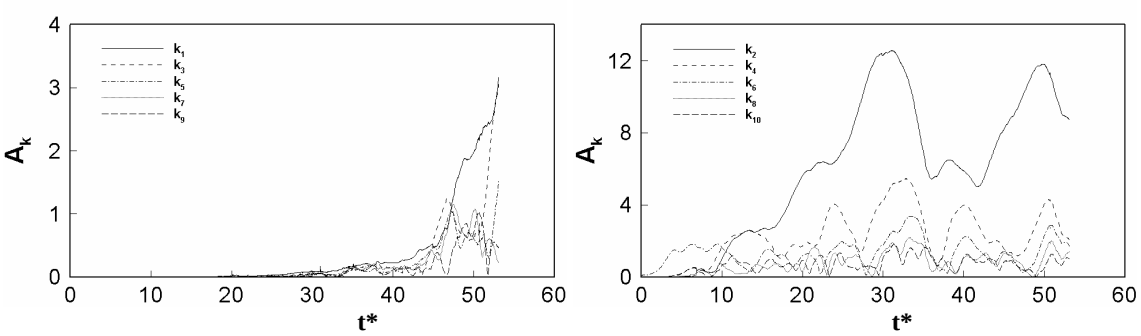

Figure 3. Amplitude of the flame front cells at different wave numbers as a function of time. The initial pressure is 5 atm; the initial disturbance at the flame front has a wave number of 6.

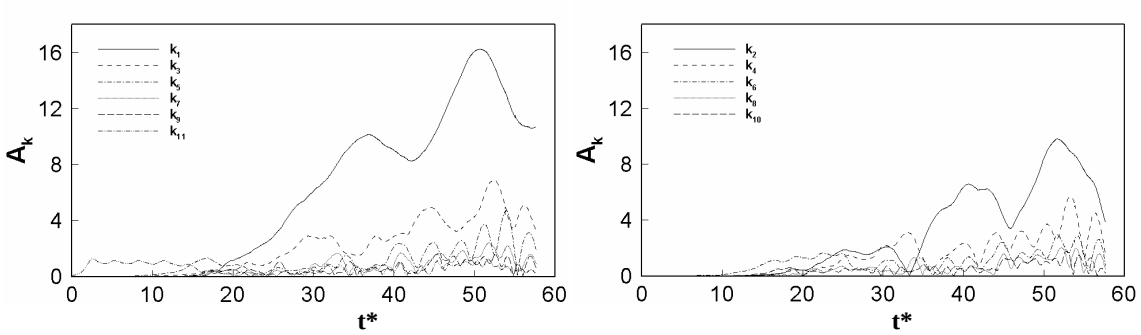

Figure 4. Amplitude of the flame front cells at different wave numbers as a function of time. The initial pressure is 5 atm; the initial disturbance at the flame front has a wave number of 11.

To examine the sensitivity of flame instability to the initial disturbance, the simulation is carried out with the initial disturbance at the flame front having a wave number of 11. The amplitude of the initial disturbance is the same as the cases discussed earlier. It appears that both the odd number of cells and even number of cells are triggered at $t^*=10$. For $t^*<10$ only the initial cells grow in amplitude. Altantzis et al. [32] reported a similar simulation using a different initial disturbance at the flame front. They showed that with 12 waves in the initial disturbance, all cells with different wave numbers were triggered at later time. The k_1 cells grew faster, and became the dominant ones after about $t^*=25$. It appears that the suppression of certain modes at the initial stage is significant only when the initial cells have long wavelengths.

Figure 5a shows further the volume integrated heat release rate in the entire computational domain for case A. The heat release rate is normalized by the heat release rate of the initial planar flame. It is clear that global heat release rate increases as the amplitude of cells at the flame front increases and as more cells are formed. During $4<t^*<30$, the heat release rate simulated using 6 waves at the initial disturbance approaches a quasi statistical stationary state, which corresponds to the quasi stationary behavior of k_4, k_6, k_8 and k_{10} modes, cf. Fig.3b. It should be pointed out that the high wave number modes contribute more to the total heat release rate, whereas large wavelength modes, e.g. k_2, contribute less. For $t^*>30$, heat release rate increases further due to the onset of odd wave number cells.

The effect of initial disturbance on the heat release rate can be seen in Fig.5a. There is considerable difference in the heat release rate for $t^*<40$, due to the difference in the evolution of odd and even wave number cells. After all modes approaching their statistical stationary states, the total heat release rate is not sensitive to the initial disturbance in the statistical sense.

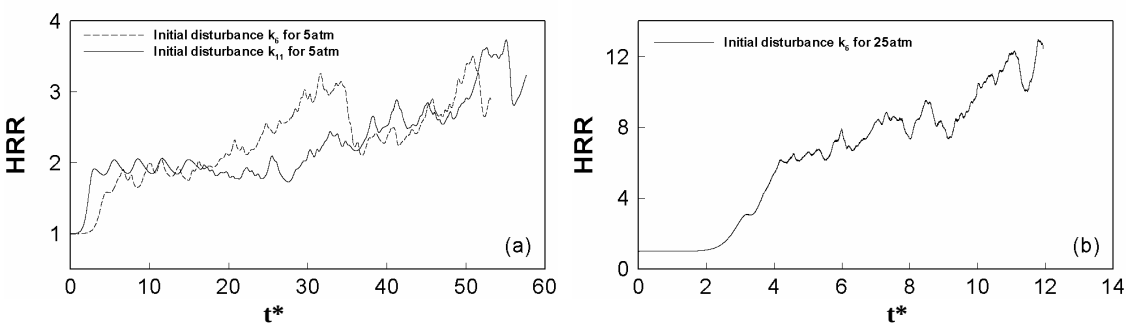

Figure 5. Total heat release rate (volume integrated in the entire domain) as a function of time. (a) case A, (b) case B. The heat release rate for each is normalized by its corresponding one in the planar flames.

Case B: lean H_2/air flame at 25 atm

At high pressures the flames are thinner, and as a result both the hydrodynamic instability and thermal-diffusive instability are enhanced. Figure 6 shows that the instantaneous distribution of OH mass fraction and temperature at several critical instances of time for the high pressure flame (case B). Figure 7 shows the amplitude of the different Fourier modes of the flame fronts. Similar to the 5 atm case (case A), there is a linear growth stage for case B until $t^*=2$. Compared to case A, the linear growth breaks down at a much short time. It is seen that at $t^*=2$, cells with wave numbers of k=2, 4, 8, 10 start to evolve, in addition to the cells of k=6. Similar to case A, the even wave number cells are triggered earlier than the odd wave number cells for the initial disturbance with k=6.

It is worth noting that at high pressure condition, case B, the small wavelength cells are more significant than the low pressure case, case A. This results in a higher global heat release rate (Fig.5b) due to the increased flame surface area, resulted from wrinkling of the small scales. It indicates that at high pressure the thermal-diffusive instability is enhanced.

One can also note that in the high pressure flames (case B) the flame front is significantly asymmetric. The fronts of the cells are inclined upwards, and there is a motion of the cells on the transverse direction. Lateral motion of cellular cells has been observed previously, e.g. [26], which is due to the higher degree of thermal-diffusive instability.

Figure 8 shows the correlation between the local heat release rate (HRR, normalized by the heat release rate of the corresponding laminar planar flame) and local flame curvature (K, normalized by the inverse of δ_L), correlation between the density-weighted displacement speed of the flame front (S_{dw}, normalized by S_L) and K, and correlation between the normal

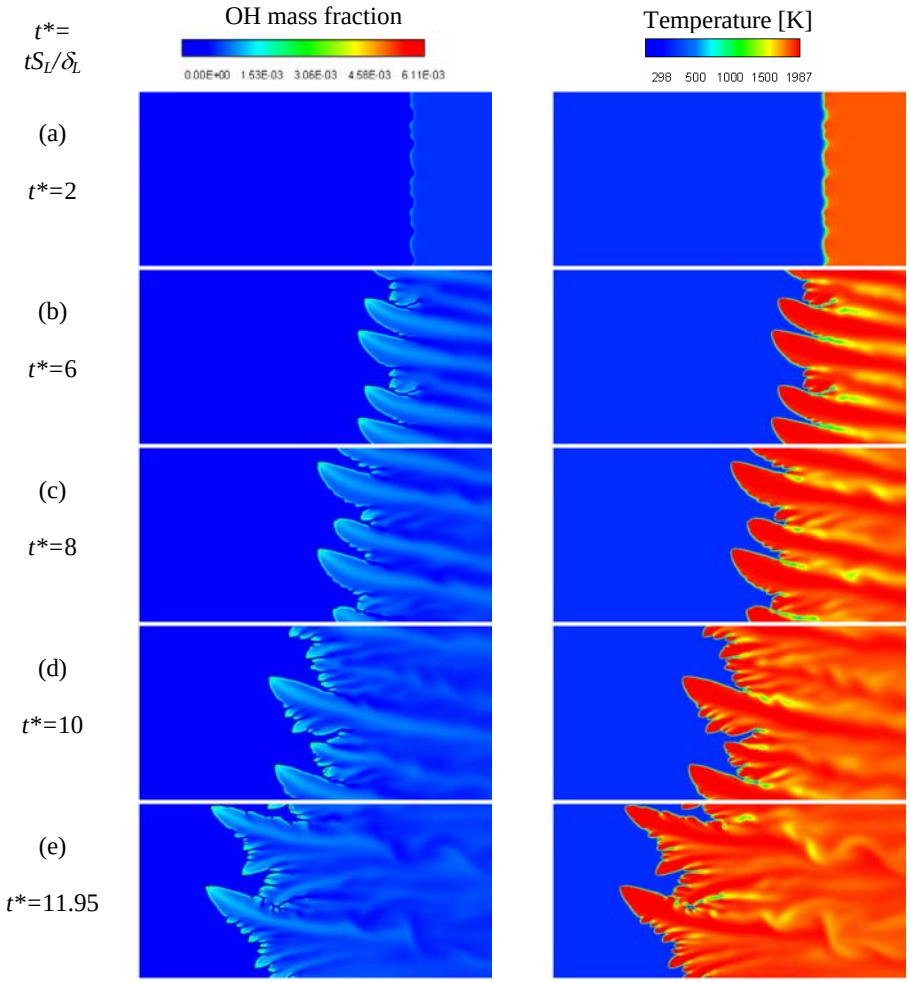

Figure 6. Instantaneous field of OH mass fraction and temperature showing five critical instances of time for case B. (a) at the end of the linear growth stage, (b) at the instance that odd number of wave cells appear, (c) at the instance that the amplitude of k_2 cells become the largest, (d) at the instance that cells with odd wave number grow rapidly.

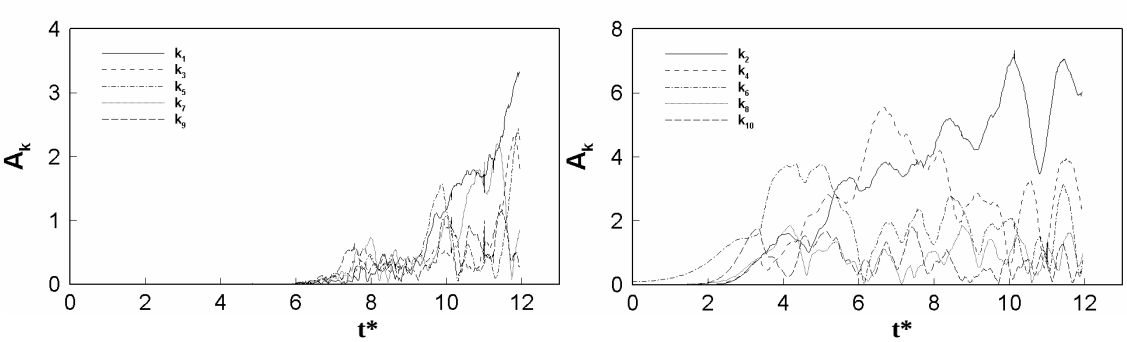

Figure 7. Amplitude of the flame front cells at different wave numbers as a function of time. The initial pressure is 25 atm and initial wave number is 6.

absolute velocity of the flame front (S_a, normalized by S_L) and K. The definition of K, S_{dw}, and S_a are taken from Ref. [32]. In general, there is insignificant correlation between HRR and K, e.g., at K close to zero, where HRR varies greatly from zero to large values. For the low pressure flames (case A) there is certain correlation between S_{dw} and K; with larger

negative curvature, S_{dw} is larger. For the high pressure flames (case B), all correlations are insignificant.

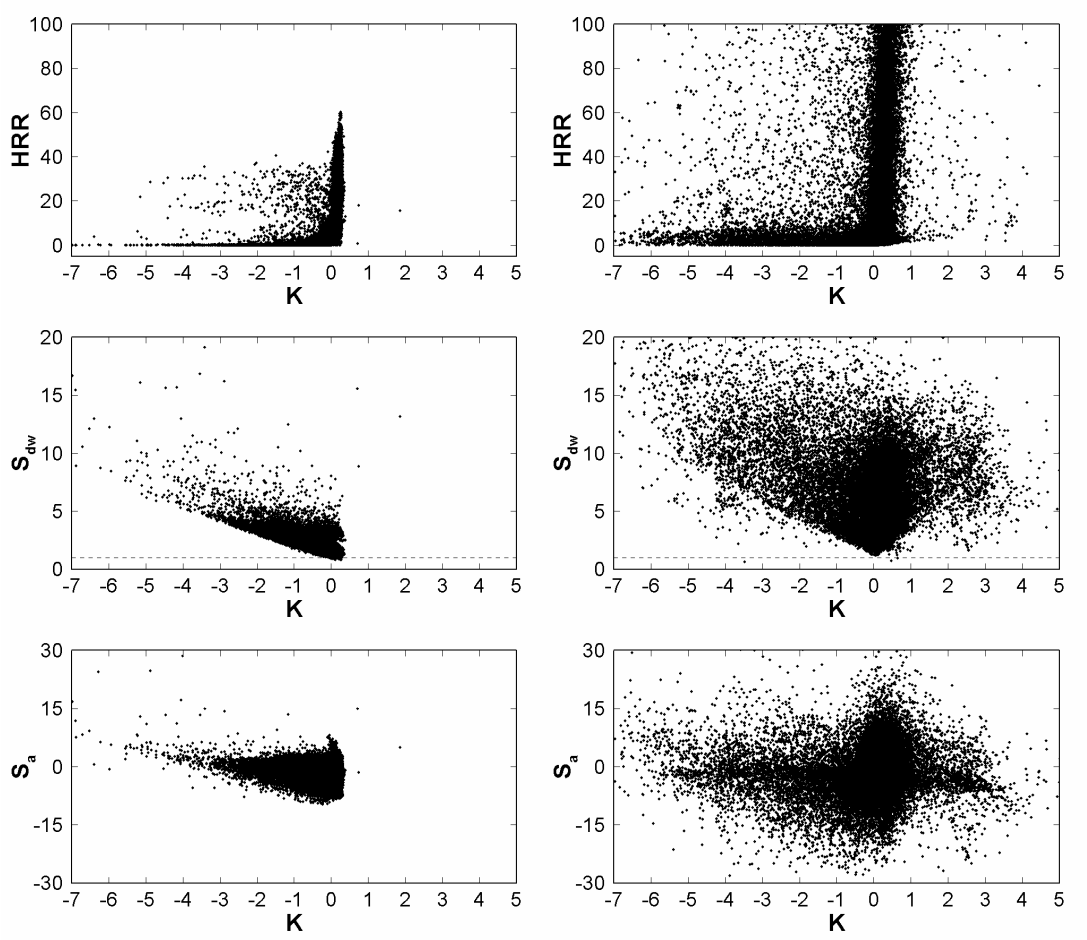

(a) 5 atm (b) 25 atm

Figure 8. Scattering of heat release rate, density-weighted displacement speed and absolute normal flame speed as functions of curvature for (a), 20<t*<53, case A, and (b) 8.5<t*<12.95, case B.

Summary

In this paper numerical simulations based on a detailed chemical kinetic mechanism and transport properties are carried out to study the linear and nonlinear evolution of a lean H_2/air premixed flames of equivalence ratio of 0.6 and pressure of 5 atm and 25 atm. The flames exhibit hydrodynamic and thermal-diffusive instabilities. It is found that evolution of flame instability in the earlier stage is rather sensitive to the initial disturbance when the length scales of the initial disturbance are not small enough. After a long time, however, when the nonlinear instability develops sufficiently, the flame front cells are shown to be in a statistical quasi stationary state. The magnitudes of the cells at different wavelengths oscillate around a statistical mean value. The mean magnitudes of longer wavelength cells are higher than the corresponding ones of the smaller wavelength cells. At the high pressure condition, the flame becomes thinner and both the thermal-diffusive instability and hydrodynamic instability are enhanced. There are more significant small wavelength cells formed in high pressure flames, leading to a higher global heat release rate due to the increased flame surface area. At low pressure conditions, there is certain correlation between the displacement speed of the flame

front and the local flame front curvature. At high pressure conditions, such correlation becomes less significant.

Acknowledgements
This work was sponsored by the Swedish Research Council (VR), the Competence Centre for Combustion Process at Lund University (KC-FP), and the national Centre for Combustion Science and Technology (CeCOST). J.F. Yu was sponsored by China Scholarship Council (CSC). The computation was performed using the computer facilities provided by the Centre for Scientific and Technical Computing at Lund University (LUNARC) and the Swedish National Infrastructures for Computing (SNIC).

References
[1] Linan, A., Williams, F.A., *Fundamental aspects of combustion*, Oxford University Press, 1993.
[2] Landau, L., "On the theory of slow combustion", *Acta Physicochim. URSS* 19: 77 (1944)
[3] Darrieus, G., "Propagation d'un front de flamme," *communication presented at La Technique Moderne*, 1938.
[4] Barenblatt, G.I., Zeldovich, Y.B., Istratov, A.G., "On diffusional-thermal stability of a laminar flame," *J. Appl. Mech. Tech. Phys.* 4: 21 (1962)
[5] Sivashinsky, G.I., "Diffusional-thermal theory of cellular flames," *Combust. Sci. Technol.* 15: 137 (1977)
[6] Markstein, G.H., *Non-steady flame propagation*, Macmillan, New York, 1964.
[7] Clavin, P., "Dynamic behavior of premixed flame fronts in laminar and turbulent flows", *Prog. Energy Combust. Sci.* 11: 1-59 (1985)
[8] Law, C. K., Sung, C. J., "Structure, aerodynamics, and geometry of premixed flamelets", *Prog. Energy Combust. Sci.* 26: 459–505 (2000)
[9] Kadowaki, S., Hasegawa, T., "Numerical simulation of dynamics of premixed flames: flame instability and vortex–flame interaction", *Prog. Energy Combust. Sci.* 31: 193–241 (2005)
[10] Matalon, M., "Flame dynamics", *Proc. Comb. Inst.* 32: 57-82 (2009)
[11] de Goey, L.P.H., van Oijen, J.A., Kornilov, V.N.,. ten Thije Boonkkamp, J.H.M, "Propagation, dynamics and control of laminar premixed flames", *Proc. Comb. Inst.* 33: 863-886 (2011)
[12] Matalon, M., Matkowsky, B.J., "Flames as gasdynamic discontinuities", *J. Fluid Mech.* 124: 239-259 (1982)
[13] Pelce, P., Clavin, P., "Influence of hydrodynamics and diffusion upon the stability limits of laminar premixed flames", *J. Fluid Mech.* 124: 219-237 (1982)
[14] Frankel, M.L., Sivashinsky, G.I., "Effect of viscosity on hydrodynamic stability of a plane flame front", *Combust. Sci. Technol.* 29: 207-224 (1982)
[15] Matalon, M., Cui, C., Bechtold, J.K., "Hydrodynamic theory of premixed flames: Effects of stoichiometry, variable transport coefficients and arbitrary reaction orders", *J. Fluid Mech.* 487: 179-210 (2003)
[16] Class, A.G., Matkowsky, B.J., Klimenko, A.Y., "Stability of planar flames as gas-dynamic discontinuities", *J. Fluid Mech.* 491: 51-63 (2003)
[17] Liberman, M.A., Bychkov, V.V., Goldberg, S.M., Book, D.L., "Stability of a planar flame front in the slow-combustion regime", *Physical Review E* 49: 445–453 (1994)
[18] Lasseigne, D.S., Jackson, T.L., Jameson, L., "Stability of freely propagating flames revisited", *Combust. Theory Model.* 3: 591–611 (1999)

[19] Sharpe, G.J., “Linear stability of planar premixed flames: Reactive Navier–Stokes equations with finite activation energy and arbitrary Lewis number”, *Combust. Theory Model.* 7: 45–65 (2003)
[20] Sivashinsky, G.I., “Nonlinear analysis of hydrodynamic instability in laminar flames – I. Derivation of basic equations”, *Acta Astronautica* 4: 1177–1206 (1977)
[21] Michelson, D.M., Sivashinsky, G.I., “Nonlinear analysis of hydrodynamic instability in laminar flames – II. Numerical experiments”, *Acta Astronautica* 4: 1207–1221 (1977)
[22] Michelson, D.M., Sivashinsky, G.I., “Thermal-expansion induced cellular flames”, *Combust. Flame* 48: 211–217 (1982)
[23] Gutman, S., Sivashinsky, G.I., “The cellular nature of hydrodynamic flame instability”, *Physica D* 43: 129–139 (1990)
[24] Bychkov, V.V., “Nonlinear equation for a curved stationary flame and the flame velocity”, *Phys. Fluids* 10: 2091-2098 (1998)
[25] Kazakov, K.A., Liberman, M.A., “Nonlinear equation for curved stationary flames”, *Phys. Fluids* 14: 1166-1181 (2002)
[26] Yuan, J., Ju, Y., Law, C.K., “Coupled hydrodynamic and diffusional-thermal instabilities in flame propagation at subunity Lewis numbers”, *Phys. Fluids* 17: 074106-1–074106-10 (2005)
[27] Kadowaki, S., Suzuki, H., Kobayashi H., “The unstable behavior of cellular premixed flames induced by intrinsic instability”, *Proc. Comb. Inst.* 30: 169-176 (2005)
[28] Sharpe, G.J., Falle, S.A.E.G., “Nonlinear cellular instabilities of planar premixed flames: numerical simulations of the Reactive Navier-Stokes equations”, *Combust. Theory Model.* 10: 483-514 (2006)
[29] Sharpe, G.J., Falle, S.A.E.G., “Numerical simulations of premixed flame cellular instability for a simple chain-branching model”, *Combust. Flame* 158: 925-934 (2011)
[30] Rastigejev, Y., Matalon, M., “Numerical simulation of flames as gas-dynamic discontinuities”, *Combust. Theory Model.* 10: (3) 459–481 (2006)
[31] Rastigejev, Y., Matalon, M., “Nonlinear evolution of hydrodynamically unstable premixed flames”, *J. Fluid Mech.* 554: 371–392 (2006)
[32] Altantzis, C., Frouzakis, C.E., Tomboulides, A.G., Kerkemeier, S.G., Boulouchos, K., “Detailed numerical simulations of intrinsically unstable two-dimensional planar lean premixed hydrogen/air flames”, *Proc. Comb. Inst.* 33: 1261-1268 (2011)
[33] Gcrar, J.F., Bell, J.B., Day, M.S., “The Soret effect in naturally propagating, premixed, lean, hydrogen–air flames”, *Proc. Combust. Inst.* 32: 1173-1180 (2009)
[34] Day, M.S., Bell, J.B., Bremer, P., Pascucci, V., Beckner, V., Lijewski, M., “Turbulence effects on cellular burning structures in lean premixed hydrogen flames”, *Combust. Flame* 156: 1035-1045 (2009)
[35] Li, J., Zhao, Z., Kazakov, A., Dryer, F.L., “An updated comprehensive kinetic model of hydrogen combustion”, *Int. J. Chem. Kinet.* 36: 566-575 (2004)
[36] Day, M.S., Bell, J.B., “Numerical simulation of laminar reacting flows with complex chemistry”, *Combust. Theory Model.* 4: 535-556 (2000)
[37] Bai, X.S., Fuchs, L., “Modeling of turbulent reacting flows past a bluff body: assessment of accuracy and efficiency”, *Computers Fluids* 23: 507-521 (1994)
[38] Gullbrand, J., Bai, X.S., Fuchs, L., “High-order Cartesian grid method for calculation of incompressible turbulent flows”, *Int. J. Numer. Meth. Fluids* 36: 687-709 (2001)
[39] Jiang, G.S., Shu, C.W., “Efficient implementation of weighted ENO schemes”, *J. Comp. Physics* 126: 202-228 (1996)
[40] Yu, R., *Large Eddy Simulation of Turbulent Flow and Combustion in HCCI Engines*, Doctoral Thesis, Department of Energy Sciences, Lund University, 2008.

[41] Peters, N., in: Peters, N., Rogg, B. (Eds.), *Reduced kinetic mechanisms for applications in combustion systems*, Lecture Notes in Physics, vol. m15, Springer-Verlag, Heidelberg, 1993, pp. 1-13.